Nuclear Instruments and Methods in Physics Research A 729 (2013) 371–380

Contents lists available at ScienceDirect

Nuclear Instruments and Methods in Physics Research A

journal homepage: www.elsevier.com/locate/nima

Efficiency calibration of x-ray HPGe detectors for photons with energies above the Ge K binding energy

Nora L. Maidana [a,*], Vito R. Vanin [a], Viktor Jahnke [a], José M. Fernández-Varea [b], Marcos N. Martins [a], Lorenzo Brualla [c]

[a] Instituto de Física, Universidade de São Paulo, Travessa R 187, Cidade Universitária, CEP:05508-900 São Paulo, SP, Brazil
[b] Facultat de Física (ECM and ICC), Universitat de Barcelona, Diagonal 645, E-08028 Barcelona, Spain
[c] NCTeam, Strahlenklinik, Universitätsklinikum Essen, Hufelandstraße 55, D-45122 Essen, Germany

ARTICLE INFO

Article history:
Received 11 April 2013
Received in revised form
6 July 2013
Accepted 8 July 2013
Available online 16 July 2013

Keywords:
X-ray detectors
HPGe detectors
Efficiency calibration
Dead layer
Seltzer model
Detector scan

ABSTRACT

We report on the efficiency calibration of a HPGe x-ray detector using radioactive sources and an analytical expression taken from the literature, in two different arrangements, with and without a broad-angle collimator. The frontal surface of the Ge crystal was scanned with pencil beams of photons. The Ge dead layer was found to be nonuniform, with central and intermediate regions that have thin (μm range) and thick (mm range) dead layers, respectively, surrounded by an insensitive ring. We discuss how this fact explains the observed efficiency curves and generalize the adopted model. We show that changes in the thickness of the Ge-crystal dead layer affect the efficiency of x-ray detectors, but the use of an appropriate broad-beam external collimator limiting the photon flux to the thin dead layer in the central region leads to the expected efficiency dependence with energy and renders the calibration simpler.

1. Introduction

HPGe detector crystals can have thick dead layers which affect their efficiency and response to photons [1–3] and can change with time [4,5]. As reported by Debertin and Helmer [6], Keyser and Hensley [7], Schláger [8] and Boson et al. [9], the thickness of these dead layers may vary considerably across the detector surface. Nonetheless, with respect to γ−ray coaxial detectors, it was found that their long-term performance is not affected, at least for energies above 100 keV, as found by Sajo-Bohus et al. [10]. They showed that the detectors used in the Euroball [10] and Gammasphere [11] experiments, despite being repaired every 500 days on an average, presented neither efficiency nor resolution losses, and sometimes even improved their performance after successive interventions.

This picture, however, does not hold for HPGe x-ray detectors. These are usually planar detectors built with very thin frontal-surface dead layers, in the micrometer range, because they are aimed at detecting photons with energies below or around 50 keV. Therefore, any variation in the dead layer thickness modifies their efficiency, but we did not find any systematic study about this phenomenon in x-ray detectors. While a dead layer of about 2 mm, common in γ−ray coaxial detectors, reduces the efficiency at 60 keV to the modest (but still significant) value of about 20% with respect to that observed for a micrometric dead layer [5], it virtually forbids the detection of photons in the 10 keV range. It is known that a guard-ring is an important requirement of planar detectors [11], in order to preserve the active region from passivation with time. Concurrently, it was demonstrated [12] that a collimator adjusted to suit the detector improves the quality of the energy spectrum and allows the determination of the efficiency from the subtended solid angle.

Efficiency calibration of x- and γ−ray detectors is commonly performed either with calibrated radioactive sources and interpolated to the required values by analytical functions using parameters fitted to the experimental points [2,6] or by Monte Carlo simulation methods [13–16]. For a planar detector, Seltzer [17] proposed an analytical formula for the detector response function that is a generalization of a single-scatter model extended to include empirical corrections to account for multiple scattering, which were guided by Monte Carlo simulation of the response for HPGe x-ray detectors with sizes spanning the range of commercially available instruments. The full-energy peak efficiency, object of this work, was obtained from the energy spectrum by integration of the part outside the peak, resulting in a calibration function

* Corresponding author. Tel.: +55 11 3091 6673; fax: +55 11 3091 6640.
E-mail addresses: nmaidana@if.usp.br, noramaidana@hotmail.com (N.L. Maidana).

0168-9002/$ - see front matter © 2013 Elsevier B.V. All rights reserved.
http://dx.doi.org/10.1016/j.nima.2013.07.033

with only two parameters: the solid angle subtended by the source and the Ge dead-layer thickness. Then, it is possible to determine the efficiency of an x-ray detector above 11 keV with the measurement of a single calibrated radioactive source like ^{57}Co, with photons at energies around 100 keV and near the Ge K binding energy, that define the solid angle and dead-layer thickness, respectively. Although this model was proposed more than 30 years ago, we were unable to find any work employing it to calibrate an x-ray detector.

In a detailed efficiency calibration of a planar HPGe x-ray detector with uncollimated radiation sources, we found that the full-energy peak efficiency did not display its typical plateau at the maximum value region, between about 30 and 80 keV [17], but presented a bump from about 70 to 110 keV. We interpret this phenomenon as a dead layer effect. It is arguable that the increase of the dead layer over time causes difficulties in the calibration procedure of Ge detectors, irrespective of the method adopted. Hence, whatever the method, a detailed knowledge of the detector is required for its efficiency calibration.

In this paper we report on the measurement of the dead layer thickness over a Ge crystal surface. The thickness of the dead layer was found to be non-uniform, with central and intermediate regions with thin (μm range) and thick (mm range) dead layers, respectively, surrounded by an insensitive ring. We discuss how this fact explains the observed efficiency curve, generalize Seltzer's model [17] to provide a good calibration function, and demonstrate that the use of a collimator leads to the expected efficiency dependence with energy and solid angle. We point out that increased dead layers show up in the detector efficiency and response functions, and the corresponding signs should be sought during the calibration procedure as a matter of routine.

2. Experimental method

The detector to be calibrated was an Ortec 1000 Series Hyperpure Germanium Low Energy Photon Spectrometer (ORTEC Advanced Measurement Technology, Oak Ridge, USA, http://www.ortec-online.com). Its data sheet states that the active Ge crystal is 25 mm in diameter and 10 mm thick, inside an Al case with diameter equal to 69.5 mm and a 0.25-mm-thick Be window. This measurement used two arrangements for the efficiency calculations, one in a broad angle and a second with a 10 mm in diameter Cu collimator. We mapped the frontal surface of the detector with photon pencil beams: a complete scan was performed with a 2 mm aperture collimator, made of Pb, and a partial scan with a 1 mm, heavy-metal collimator.

2.1. Crystal position

The detector size and its position relative to the end cap can be found with x-ray images [3,9] as shown in Fig. 1, which was obtained with a Philips Highly Stabilized x-ray system MG 225/450. The detector was placed at 3.20 m from the x-ray system window. The plate was located behind the detector, at 20.5 cm from the axis of the Al case. The operating conditions to acquire the image were 50 kV and 10 mA during 30 s. The plate was read in an Agfa digitizer type 5175/100 CR-30.

2.2. Arrangement and efficiency calibration

Calibrated ^{133}Ba, ^{152}Eu, ^{207}Bi and ^{241}Am radioactive sources purchased from Amersham, as well as ^{57}Co and ^{137}Cs calibrated x-ray sources from LMN–IPEN/CNEN-SP (Laboratório de Metrologia Nuclear–Instituto de Pesquisas Energéticas e Nucleares, Comissão Nacional de Energia Nuclear, São Paulo) were used to include

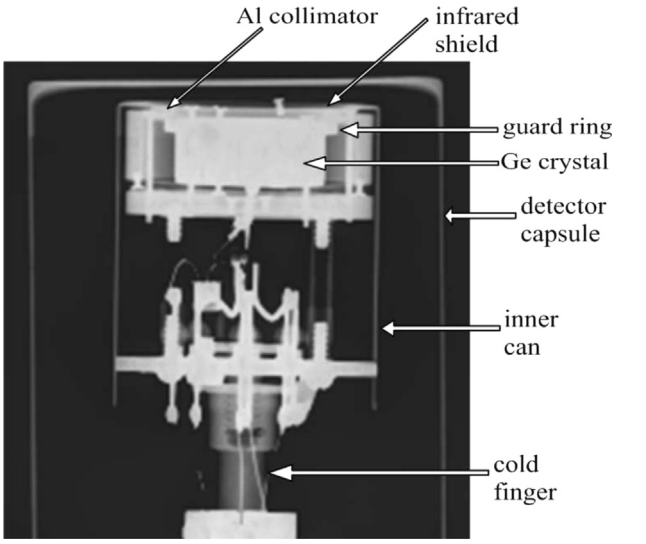

Fig. 1. Image obtained with an x-ray system showing the detector top-hat shape with a 2-mm guard-ring. The detector capsule, which keeps the crystal in vacuum, is the most external enclosure. The crystal and the capsule axes misalignment can also be observed. The infrared shield cannot be seen; the arrow with this label points to its position.

additional calibration points between 13 and 136 keV. The decay data required for the efficiency determination were taken from [18], except for the ^{207}Bi half-life, adopted from [19]. The experimental arrangement was that employed in the on-line measurement of inner-shell ionization cross-sections by electron impact with the São Paulo Microtron injector [20]. The sources were placed, at the target position, inside an irradiation chamber with a 50−μm Al spectroscopy window 299.5(7) mm away from the detector end cap. The detector was shielded with Cu and surrounded by Pb bricks to minimize the background detection. The efficiency curve obtained with this arrangement showed a bump around 80 keV, as pointed out in the Introduction. Since the experiment required an accurate efficiency calibration in the 60–100 keV energy interval, a ^{198}Au, 99.99% pure metallic source prepared by neutron activation (mass thickness equal to 20 mg/cm^2) was activity-calibrated by LMN–IPEN/CNEN-SP to provide another point at the bump region to improve the information about the energy dependence. This radionuclide decays by β^- to ^{198}Hg with a half-life of 2.7 days and a 412-keV γ transition that produces Hg characteristic x-rays after internal conversion [18]. The only usable x-ray peak from this source was Hg $K\alpha_1$, because Hg $K\alpha_2$ and Hg Kβ are mixed with the Au K x-rays from fluorescence induced by electron-impact ionization caused by the β^- emitted in the decay of ^{198}Au.

In a second stage, we followed Martin and Burns [12] and added a cylindrical collimator made of Cu, 70-mm long with a 10-mm aperture aligned with the Ge crystal, placed 5 mm away from the detector Be window, and observed the expected efficiency energy dependence, as described below. The detector capsule was tilted with respect to the collimator axis to adequately compensate for the aforementioned misalignment of the crystal with respect to the capsule.

The full-energy peak efficiency P_i at photon energy E_i was determined from the corresponding net peak area a_i in the observed spectrum [2,6]:

$$P_i = \frac{a_i}{A_s I_i \Delta t}, \tag{1}$$

where I_i is the intensity (yield) of the corresponding γ- or x-ray transition in the decay of radioactive source s with activity A_s in a counting time Δt. The net peak areas were obtained from the total number of counts above the continuum part of the spectrum in the peak region minus the contribution from the components of the

response function that extend under the full-energy peak. This correction ranges from 1.5% to 2.5% of the total peak areas in the uncollimated arrangement and is negligible with the collimator included in the experimental setup.

Absorption of photons in the source case of ^{133}Ba, ^{152}Eu and ^{241}Am sources was corrected, as well as small differences in source position in the holder. The combination of both effects changed the experimental efficiencies by less than 2.2% for all photon energies. Besides the source case and the detector Be window, the absorption layers considered were 50 μm Al irradiation chamber spectroscopy window, 3.3 mg/cm^2 aluminized Mylar (the infra-red reflector inside the detector capsule), and 300 mm of air, although only the Al foil played a significant role in the attenuation of photons in the energy interval of interest. The relative uncertainties in these values are of a few percent and the crystal dimensions were checked against the detector radiography.

Notice that most of the employed radionuclides are multiple-line standards, leading to correlations between the experimental efficiencies evaluated at energies corresponding to transitions from the same source. The ensuing covariance matrix was taken into account in the least-squares parameter fit procedure as it will be detailed in Section 4.

2.3. Efficiency mapping

The efficiency of the detector to photons impinging on different regions of the crystal surface was determined from measurements with collimated ^{241}Am and ^{152}Eu sources in an arrangement similar to that used by Boson et al. [9]. Sources and collimator were placed on an x–y table capable to scan the entire crystal frontal surface over a grid of 3×3 mm^2 with an incident angle of 90° with respect to the crystal frontal surface and also to take measurements at 45° incidence. The 45-mm-thick Pb collimator, with an aperture of 2 mm, was placed at 7 mm from the detector Be window.

2.4. Dead layer thickness measurement

The dead layer thickness at the center of the detector frontal surface was determined from a few measurements of the 14 keV x-ray from a ^{241}Am source, viewed through the 2-mm aperture collimator described in the preceding section, with 90° and 45° incidence near the center of the crystal [9]. Dead layer thicknesses in other points of the frontal surface were deduced from ratios between peak areas of photons of the same transition from collimated sources at normal incidence in different locations, as will be explained. Differential attenuation was not used to evaluate the dead layer thickness, because the small-aperture Pb collimator may have minute irregularities that make corrections for absorption and elastic scattering in the inner wall prone to error.

It will be shown that the values obtained by this procedure were not sufficiently accurate for a good efficiency calibration. Nevertheless, they were important to understand the detector characteristics and for delineating its schematic model, summarized in Fig. 2, whose development is described below.

In the normal-incidence measurements over the crystal surface with the collimated ^{241}Am source, the number of counts in the 14 and 59 keV peaks displays two distinct behaviors. Their ratio is fairly constant over the central half of the frontal surface, while both peaks disappear over the outer half, up to the crystal rim. From the fact that the attenuation coefficients of Ge for 14 and 59 keV photons are 600 and 10 cm^{-1}, respectively, it can be deduced that the dead layer is very thin in the central part, in the micrometer range; and thick, in the millimeter range, in the annular area where both γ rays are missing in the observed spectra. We shall, therefore, call 'central region' the area corresponding to the set of points that

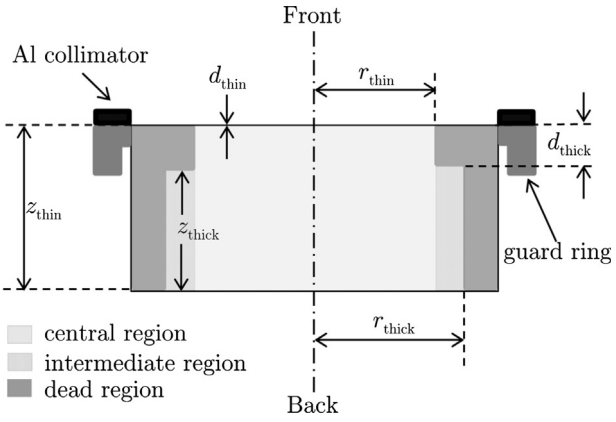

Fig. 2. Sketch of the detector crystal, cut through a crystal diameter along its cylindrical symmetry axis. The active and inactive regions are light and dark gray, respectively. Figure not to scale.

are sensitive to the ^{241}Am photons, and identify its radius as $r_{\rm thin}$. This active region, which is sensitive to x-rays, is covered by a thin dead layer of thickness $d_{\rm thin}$.

A different picture was seen with the 40 and 122 keV photons from the ^{152}Eu source. The ratio between the number of counts in the corresponding peaks varied in a large range of values in the spectra taken with the pencil beam hitting different points of the crystal surface. Moreover, in some spectra the 40 keV peak disappeared while the 122 keV photons gave a prominent peak, but the crystal peripheral region responded neither to 40 nor to 122 keV photons. Hence, the region sensitive to 122 but not to 40 keV photons will be called 'intermediate region', characterized by a 'thick dead layer'. Pixels where both transitions were seen, but with the 40 keV x-rays attenuated, must have partially covered this intermediate region, which allows the deduction of an upper limit for its dead layer thickness, using the algorithm described below.

From spectra taken for the same live time interval, we calculated for each photon energy and for each pixel i the ratio of the number of counts in the peak, $A_{E,i}$, to its average value in the thin dead layer region $\langle A_{E,c}\rangle$:

$$R_{E,i}=\frac{A_{E,i}}{\langle A_{E,c}\rangle}. \tag{2}$$

Assuming that the 40 keV x-rays are completely absorbed by the thick dead layer, the fraction of the pixel i covered by the thick dead layer is

$$F_i=1-R_{40,i}. \tag{3}$$

We are interested in pixels where $F_i\sim0.5$, meaning that they were located over the boundary between the central and intermediate regions. The number of 122 keV photons counted in one of these frontier pixels, $A_{122,i}$, is the sum of two components, that we call $A^{\rm thin}_{122,i}$ and $A^{\rm thick}_{122,i}$ according to the crystal region, central or intermediate. The number of counts from photons that reach the central region can be deduced from the average value in that region as

$$A^{\rm thin}_{122,i}=\langle A_{122,c}\rangle(1-F_i)=\langle A_{122,c}\rangle R_{40,i}. \tag{4}$$

The balance must be due to photons that hit the intermediate region,

$$A^{\rm thick}_{122,i}=A_{122,i}-\langle A_{122,c}\rangle R_{40,i}. \tag{5}$$

Dividing this expression by the number of photons detected in the thin dead layer region in the same area, $\langle A_{122,c}\rangle F_i$, we obtain

$$\frac{A^{\rm thin}_{122,i}}{\langle A_{122,c}\rangle F_i}=\frac{R_{122,i}}{F_i}-\frac{R_{40,i}}{F_i}=\frac{R_{122,i}-R_{40,i}}{1-R_{40,i}} \tag{6}$$

which represents the combined effect of attenuation of the 122 keV photons due to the thick dead layer with the intrinsic efficiencies in the intermediate and central regions. However, the hypothesis that the photons hit only the central and intermediate regions may not be valid when the intermediate region is narrower than the region examined with the collimated radioactive source, and so some of the photon flux can impinge on the outer ring, completely unresponsive to photons. It turned out that the intermediate region in our case is less than 2 mm wide, while we scanned the surface with a 3 mm resolution grid. Therefore, the experimental value given by formula (6) should be regarded as an underestimation of the ratio of the efficiency at 122 keV in the intermediate region to that in the central region. Since the detection efficiency can be related to the dead layer thicknesses, as detailed in the next section, this measurement provides just an upper limit for its size in the intermediate region.

These findings suggest a sharp change in dead-layer thickness from the central to the intermediate regions. However, the 2 mm resolution of this collimator was insufficient to draw this conclusion reliably. Thus, we scanned the crystal frontal surface along a few lines with a heavy metal collimator (95% W and 5% Cu plus Ni, manufactured by Brassinter S.A., São Paulo, SP, Brazil) 45 mm in length and 1 mm in diameter, in steps of 1 mm, using a ^{241}Am source.

With the spatial resolution obtained with this collimator, it was possible to find a spot where a weak 59 keV peak was observed, but the 14 keV peak was absent, giving another way to assess the intermediate region dead-layer thickness. In the assumption that the photon beam impinges only in the intermediate region, when scanning point k, we can assume that

$$A_{59,k} = \langle A_{59,c}\rangle \exp[-\mu_{\mathrm{Ge},59\ \mathrm{keV}}(d_{\mathrm{thick}} - d_{\mathrm{thin}})]. \tag{7}$$

These measurements allowed us to get some information about the slope of the dead-layer thickness change from the central to intermediate regions. The developed model is described and discussed in the Appendix, along with all the related data.

3. Analytical efficiency model

The energy dependence of the x-ray detector efficiency for detection in the full-energy absorption peak at the large source-to-detector distance of this experiment can be described by (*i*) losses in the detector capsule and other materials between the source and the detector, (*ii*) a function that accounts for absorption in the active volume corrected for the escape of inelastically scattered photons, and (*iii*) Ge K x-ray escape [17,21].

Seltzer [17] developed an analytical model for pin-hole collimated photon beams that accounts for the escape of K x-rays and photons scattered once or twice inside the active detector volume. He checked the accuracy of the model against experimental and simulated results and showed its usefulness also for broad-beam sources. Using mostly the notation of Seltzer [17], for a photon of energy E, the full-energy peak efficiency P of a detector with a Ge crystal of thickness z and radius r is given by

$$\begin{aligned} P(E;z,r) &= \frac{\Omega}{4\pi}\, T(E)\left\{1-\exp[-\mu_{\mathrm{Ge}}(E)z]-P_{X\alpha}(E)-P_{X\beta}(E)-\int C(E,\epsilon;z,r)\,\mathrm{d}\epsilon\right\} \\ &= \frac{\Omega}{4\pi}\, T(E)\, p(E;z,r) \end{aligned} \tag{8}$$

where $T(E)$ stands for the transmission through the path between the source and the Ge crystal, $\mu_{\mathrm{Ge}}(E)$ for the linear attenuation coefficient of photons of energy E in Ge excluding coherent scattering, $P_{X\alpha}(E)$ and $P_{X\beta}(E)$ for the escape probabilities of Ge Kα and Kβ x-rays, respectively, and $C(E,\epsilon;z,r)$ for the probability that a photon of energy E deposits an energy ϵ in the detector active volume; Ω is a normalization factor that accounts for the solid angle covered by the detector with respect to the radioactive source. Furthermore, Eq. (8) also defines the intrinsic peak detection efficiency $p(E;z,r)$, which corresponds exactly to the function $P_{\mathrm{f}}(E,z,r)$ isolated from formulas (7) and (8) of Ref. [17].

The x-ray escape probabilities admit analytical expressions [22,17]; here we adopt that of Seltzer [17] as follows:

$$P_{X\tau} = \frac{1}{2}\omega_{\mathrm{K}} p_\tau q_{\mathrm{K}}(E)\frac{\mu_{\mathrm{PE}}(E)}{\mu_{\mathrm{Ge}}(E)}\left[1-\frac{\mu_{\mathrm{Ge}}(E_\tau)}{\mu_{\mathrm{Ge}}(E)}\right]\ln\left[1+\frac{\mu_{\mathrm{Ge}}(E)}{\mu_{\mathrm{Ge}}(E_\tau)}\right] \tag{9}$$

where τ is either α or β, therefore the quantities E_τ and p_τ represent, respectively, the Kα or Kβ x-ray energy and relative emission probability; ω_{K} is the Ge K fluorescent yield, $q_{\mathrm{K}}(E)$ is the fraction of photoelectric absorption events that occur in the K shell, and $\mu_{\mathrm{PE}}(E)$ is the attenuation coefficient for photoelectric absorption of photons of energy E in Ge. The sum $P_{X\alpha}+P_{X\beta}$ amounts to a maximum of 16% of the incident photons at Ge K binding energy and falls almost exponentially with energy, reducing to 0.6% for 60 keV photons.

The analytical formula for $C(E,\epsilon;z,r)$ accounts for single and double inelastic scattering in the detector crystal. Although based on the analytical calculation of the transmission of photons through the disc-shaped crystal, Seltzer [17] introduced corrections obtained by Monte Carlo simulations by means of a few parameters added to the analytical function to get better agreement with the simulations. This function was developed to provide the detailed detector response function with the deposited energy ϵ, which is not needed to obtain the full-energy peak efficiency. Therefore, we just integrate numerically $C(E,\epsilon;z,r)$ from 0 to the maximum deposited energy to quantify the escape probability of photons that undergo inelastic interactions in the crystal active volume. This integral is very small in the range dominated by K x-ray escape, amounting to less than 1% for 60 keV photons. Its dependence is weak on crystal radius at all energies, while the crystal length becomes increasingly important for energies above 100 keV. For a Ge crystal of thickness equal to 10 mm, 10% of the 130 keV photons that hit the crystal surface escape its volume.

The model can be generalized if we factorize the transmission through the Ge dead layer thickness d from the first factor in $T(E)$, which can be written as

$$T(E) = T_0(E)\exp[-\mu_{\mathrm{Ge}}(E)d] = \left\{\prod_{i=1}^{n}\exp[-\mu_i(E)t_i]\right\}\exp[-\mu_{\mathrm{Ge}}(E)d] \tag{10}$$

where n different layers of absorbers with uniform thicknesses t_i and corresponding linear attenuation coefficients $\mu_i(E)$ are accounted for by the factor $T_0(E)$.

Seltzer's formula can be generalized to the case where ν zones characterized by different dead layers with thicknesses d_η coexist in the detector, each one subtending a solid angle Ω_η:

$$P(E;\boldsymbol{\Omega},\mathbf{d}) = T_0(E)\sum_{\eta=1}^{\nu}\frac{\Omega_\eta}{4\pi}\exp\left[-\mu_{\mathrm{Ge}}(E)d_\eta\right]p\left(E;z_\eta,r_\eta\right) \tag{11}$$

where $\boldsymbol{\Omega}=\{\Omega_1,\ldots,\Omega_\nu\}$ and $\mathbf{d}=\{d_1,\ldots,d_\nu\}$ represent the sets of solid angles and dead layer thicknesses of the detector zones, respectively, whereas z_η and r_η are the corresponding thicknesses and radii. Since $z_\eta+d_\eta$ is the known detector length, only one of these parameters must be fitted, and we chose to fit the dead-layer thicknesses. In the assumption of cylindrical symmetry, the different zones are concentric, therefore the radii r_η are related to the solid angle parameters by $r_\kappa^2 = 4\rho^2\sum_{\eta=1}^{\kappa}\Omega_\eta$ when we number the zones from the center to the periphery of the crystal. However, the efficiency in this model is almost insensitive to r_η, hence they can be fixed at values compatible with the fitted values

of $\boldsymbol{\Omega}$, which makes the least-squares procedure easier to apply. Therefore, the parameters that must be fitted to the experimental data once the n absorber materials and their thicknesses are known are only $\boldsymbol{\Omega}$ and $\mathbf{d}$.

Using this model, the peak-area ratio of formula (6), which represents the relative detection efficiency between the different detector zones, can be calculated by

$$\frac{\epsilon_{\text{thin}}(E)}{\epsilon_{\text{thick}}(E)} = \frac{\exp[-\mu_{\text{Ge}}(E)d_{\text{thin}}]p(E;z_{\text{thin}},r_{\text{thin}})}{\exp[-\mu_{\text{Ge}}(E)d_{\text{thick}}]p(E;z_{\text{thick}},r_{\text{thick}})} \tag{12}$$

where the quantities d, z, and r are indexed as 'thin' or 'thick' according to the crystal region, central or intermediate, respectively, as defined in Section 2.4.

The attenuation coefficients in the efficiency model, formulas (8)–(12), were taken from the National Institute of Standards and Technology (NIST) database [23].

4. Least-squares procedure for efficiency calibration

The parameters of the efficiency function given by Eq. (11) were fitted to the experimental data by the least-squares method, taking into account the correlations between the experimental values due to the use of more than one line from the same calibrated radioactive source. In this section, we shall solve the least-squares equation in a way that helps checking the sensitivity of the method to the dead layer thickness.

Given a set of experimental full-energy peak efficiency values $\{(E_i,P_i), i=1,\ldots,N\}$, where N is the number of data points, the merit function to minimize is written as follows:

$$Q(\boldsymbol{\Omega},\mathbf{d}) = \mathbf{q}^t\mathbf{V}^{-1}\mathbf{q} \tag{13}$$

with the components of the column vector of residues $\mathbf{q}$ given by

$$q_i = P_i - P(E_i;\boldsymbol{\Omega},\mathbf{d}) \tag{14}$$

and the elements of the data variance matrix $\mathbf{V}$ by [24]

$$V_{ij} = P_iP_j\left\{\left[\frac{\text{var}(a_i)}{a_i^2}+\frac{\text{var}(I_i)}{I_i^2}\right]\delta_{ij}+\frac{\text{var}(A_s)}{A_s^2}\delta_{s(i),s(j)}\right\} \tag{15}$$

where var(x) stands for the variance of quantity x and δ_{ij} are Kronecker deltas. Thus, the only non-diagonal terms correspond to data coming from the same source, $s(i)=s(j)$. Notice that in Eq. (11) the factors $T_0(E)$ and $p(E;z_\eta,r_\eta)$ do not have any adjustable parameter, hence $P(E_i;\boldsymbol{\Omega},\mathbf{d})$ is linear in the parameters $\boldsymbol{\Omega}$ and nonlinear in the parameters $\mathbf{d}$. The least-squares minimization procedure can be performed assigning values to the non-linear parameters $\mathbf{d}$ and calculating the remaining linear parameters $\boldsymbol{\Omega}_d$, which does not require an iterative procedure. When $\mathbf{d}$ has one or two components, it is possible to map the sum of residues Q against the set of values $\mathbf{d}$ used, providing a one- or two-dimensional plot to assess the fit: we keep guessing $\mathbf{d}$ until the minimum of Q can be seen in the plot. Hence, we plot $Q(\boldsymbol{\Omega}_d,\mathbf{d})$ as a function of $\mathbf{d}$, where $\boldsymbol{\Omega}_d$ are the values that minimize Q for a given $\mathbf{d}$. Since our detector has a single zone when using the collimator and two zones without the collimator, the least-squares procedure can be summarized in one- or two-dimensional plots in coordinates corresponding to the nonlinear parameters. The variance matrix of the parameters $\boldsymbol{\Omega}$ and $\mathbf{d}$ is calculated from the variance matrix of Eq. (15) and the design matrix $\mathbf{X}$ by

$$\mathbf{V}_{\boldsymbol{\Omega}\mathbf{d}} = (\mathbf{X}^t\mathbf{V}^{-1}\mathbf{X})^{-1} \tag{16}$$

where

$$X_{i\kappa} = \frac{\partial P(E_i,\boldsymbol{\Psi})}{\partial\psi_\kappa}\Big|_{\hat{\boldsymbol{\Omega}},\hat{\mathbf{d}}} \tag{17}$$

and $\boldsymbol{\Psi}$ is the union of the parameters $\boldsymbol{\Omega}$ and $\mathbf{d}$; ψ_κ denotes each of its components, that is, $\psi_\kappa\in\{\Omega_1,\ldots,\Omega_\nu,d_1,\ldots,d_\nu\}$ with ν the number of zones. $\hat{\boldsymbol{\Omega}}$ and $\hat{\mathbf{d}}$ denote the fitted values of $\boldsymbol{\Omega}$ and $\mathbf{d}$, respectively.

5. Results

5.1. Detector structure and dead layer thicknesses from photon attenuation

The x-ray images of the detector allowed us to verify that the crystal and capsule axes were not properly aligned. The crystal axis crossed the frontal capsule surface about 3 mm away from the capsule axis.

From the measurements with the collimated photon beams with normal and 45° incidence on the detector's frontal surface, described in Section 2.3, we measured the dead layer thickness in the center of the crystal as 1.2(6) μm. From the constancy of the 14/59 keV intensity ratio in the central region we concluded that the thin dead layer is very homogeneous over the whole central region. We also found that the detector rim was completely insensitive, and observed an intermediate region with a thick dead layer. It should be clear that these regions refer to the visible diameter and exclude the guard-ring that lies below the Al collimator, the latter barely visible in Fig. 1.

Following the procedure described in Section 2.4 with the 40 and 122 keV photons from ^{152}Eu, the experimental value obtained with formula (6) can be substituted in the right-hand side of Eq. (12), which, neglecting the effect of d_{thin} at the energy of interest, is a function of d_{thick} only. Solving this equation we found that $d_{\text{thick}} \leq 3$ mm; the complete set of values is given in the Appendix.

Fig. 3 shows the 14- and 59-keV peak areas along one of the lines on the crystal surface scanned with the narrow collimator, where an apparently sharp step in the dead-layer thickness can be observed; similar results were obtained in the other two lines scanned. In all the spectra corresponding to the pencil photon beams impinging in the central region and also in its frontier with the intermediate region, where the 14 keV peak was seen, the 14 keV to 59 keV peak area ratio was the same. From Eq. (7), using the 59 keV peak area in the point corresponding to position 10 mm in the figure, it was obtained as $d_{\text{thick}}\approx 3.5$ mm; the complete set of values obtained with the points that may have fallen on the intermediate region is given in the Appendix.

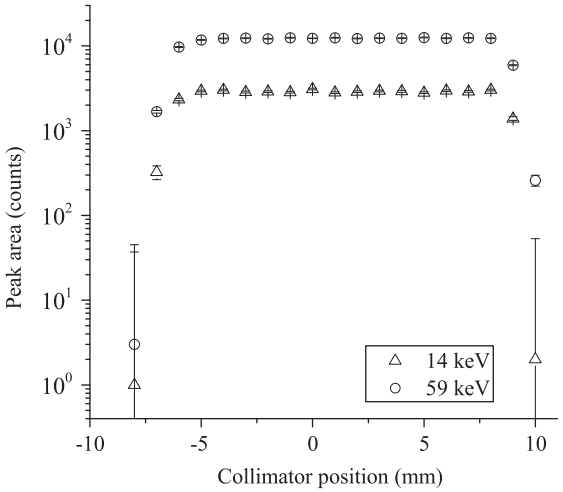

Fig. 3. Peak areas of the 14- and 59-keV transitions from ^{241}Am (lower and upper points, respectively) along one line on the crystal surface scanned with the narrow collimator. The abscissa indicates relative positions along that line.

All the experimental findings from the detector scanning are summarized in the schematic model depicted in Fig. 2, with the crystal divided in three regions: the central region with a thin dead layer that is sensitive to low-energy photons, an intermediate region with a thick dead layer that responds only to photons with energies above 60 keV approximately, and an outer dead ring unable to detect photons.

5.2. Evaluation of dead layer thicknesses and the active volume

We start with the efficiency in the broad-angle collimated source arrangement described in Section 2.2, which was designed to select only the photons that can enter the detector active volume through the central region, where the crystal has a thin dead layer. Since all the other absorbing layers have known thicknesses, the fit parameters are just the subtended solid angle Ω defined by the collimator and d_{thin}, the dead layer thickness in the central region. Hence, the least-squares procedure consists in finding the minimum of the function $Q(\Omega_d, d)$ from formula (13), plotted in Fig. 4. The well-pronounced minimum at $d_{\text{thin}} = 2.04$ μm with $\chi^2 = 7.6$ and 15 degrees of freedom suggests that the dead layer thickness can be estimated accurately from this measurement. Using in Eq. (16) the values of the fitted solid angle $\hat{\Omega}$ and dead layer thicknesses d_{thin}, we found 0.16 μm for the standard deviation of d_{thin}. Fig. 5 displays the experimental efficiencies along with the calibration curve. When fitting the parameters of the efficiency model (Ω and d_{thin}) to the experimental data obtained with ^{57}Co only (γ-rays of 14-, 122- and 136-keV), the obtained values are compatible with those shown above, but with doubled standard deviations, because of the reduced statistical information. The differences in the calculated efficiencies are smaller than 1% for all energies in the range of interest.

The efficiency model for the uncollimated source arrangement is given by formula (11) with two zones, one with a thin dead layer in the micrometer range, and another with a thick dead layer in the millimeter range. We adopted for the thin dead layer the value from the collimated detector calibration, $d_{\text{thin}} = 2.04(16)$ μm. Hence, we fitted three parameters, namely d_{thick}, Ω_c and Ω_p, the last two representing the solid angles covered by the central and intermediate regions, respectively, and collected in the vector $\boldsymbol{\Omega}$ of Eqs. (13), (14), (16) and (17). Since the model is linear in $\boldsymbol{\Omega}$, it is possible to plot the sum of the residues $Q(\boldsymbol{\Omega}_d, d)$ as a function of d, see Fig. 6, and its minimum gives the least-squares estimate $d_{\text{thick}} = 2.3(4)$ mm with $\chi^2 = 19$ (15 degrees of freedom). Fig. 7 shows the experimental efficiency values along with the fitted calibration curve, represented by the continuous curve, which corresponds to the sum of two regions with different dead layers; these components are plotted as dashed curves. The values obtained for the solid angle parameters correspond to radii of the central and intermediate regions equal to 8.02(4) mm and 9.28 (18) mm, respectively.

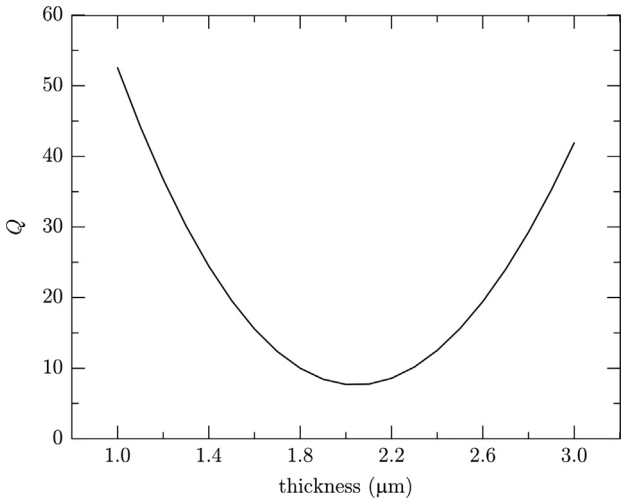

Fig. 4. Plot of $Q(\Omega_d, d)$ for the determination of d_{thin}.

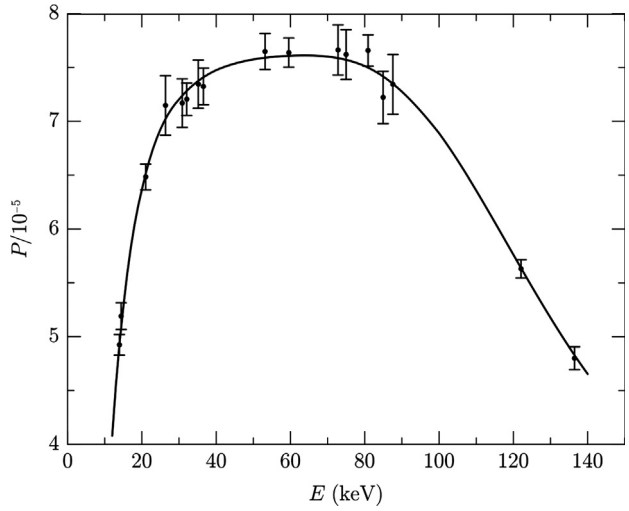

Fig. 5. Efficiency of the collimated detector as a function of photon energy. The circles are experimental values, and their uncertainty bars correspond to one standard deviation. The maximum value corresponds to 0.97 of the solid angle subtended by the collimator.

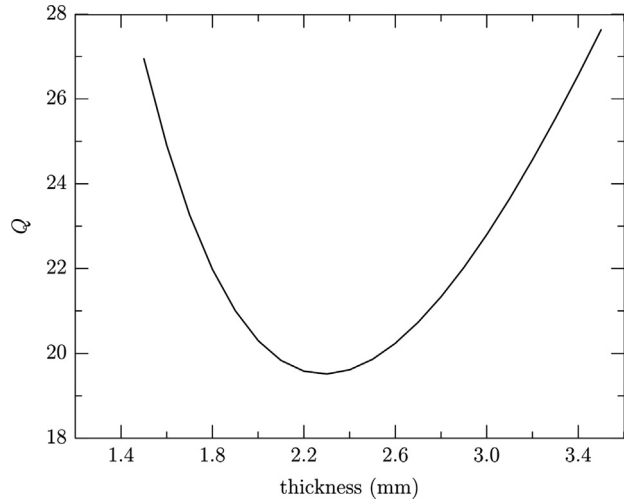

Fig. 6. Plot of $Q(\boldsymbol{\Omega}_d, d)$ for the determination of d_{thick}.

6. Discussion

We did not find, for x-ray detectors, any systematic study of the dependence of Ge dead layer thickness with age or incidents that may affect the relatively small planar crystal, like capsule vacuum loss or crystal warming. However, all the papers that report measurement or evaluation of Ge dead layer thickness on large detectors state a value smaller than or about 2 mm, independently of the detector age or the reason that led to the development of the dead layer; these reports refer to γ−ray detectors, which are Ge crystals with frontal surfaces measuring tens of cm^2, where thicker dead layers in small regions like the one observed here, covering about 1 cm^2, will not harm the overall detector response. Moreover, it was already pointed out by Vetter in a review work

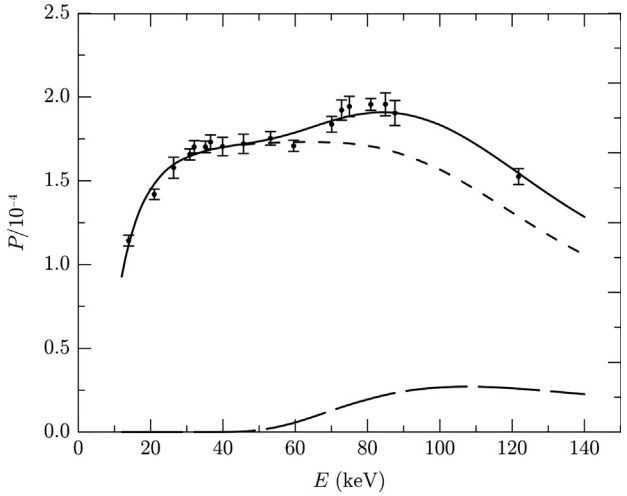

Fig. 7. Efficiency of the uncollimated detector as a function of photon energy. The circles are experimental values, and their uncertainty bars correspond to one standard deviation. The fitted calibration curve is shown by the continuous curve and its components with different dead layers by the dashed lines. The expected efficiency curve for a detector with the same diameter and responsive to low-energy photons in its entire surface can be obtained by multiplying the thin dead layer efficiency by a factor of about 2.

[11] that "planar detectors still require guard-rings of the order 3–10 mm to separate performance-degrading surface effects from the sensitive detection volume", which means that it is expected that the dead layer can become larger than observed here. Therefore, the thick dead layer measured in our HPGe detector is not unusual.

The simplest sign of the dead layer thickening process in an x-ray detector seems to be the maximum efficiency value, which according to Martin and Burns [12] should be between 0.92 and 0.96 times the solid angle. The analytical model of Seltzer gives values between 0.96 and 0.98 for detectors whose crystal diameters are in the range from 2 to 16 mm and thicknesses between 7 and 13 mm, with Be windows less than 0.5-mm thick and dead layer thicknesses less than 12 μm, actually covering the range of commercially available equipments. The maximum efficiency value for our detector, with collimated sources, corresponds to about 0.97 of the solid angle accepted by the collimator, which is about half of the solid angle subtended by the total crystal circular area.

The use of a collimator requires good knowledge of the crystal position inside the capsule, which was determined from the x-ray image shown in Section 2.2; the relatively small dimensions of crystal detectors for low-energy photons make the radiographic plate more important for them than for the larger coaxial γ−ray detectors. Signs of dead layer development in the spectrum shape and the geometrical efficiency that correspond to increased peak tails and increased number of events out of the full-energy peak were already discussed by Martin and Burns [12]. Here, we focused on the consequences on the efficiency calibration curve and, with the help of Seltzer's analytical model for the efficiency of planar detectors [17], succeeded in explaining quantitatively its peculiar shape. Notice that even the extensive scan of the detector frontal surface with radioactive sources did not produce sufficiently detailed information about the dead layer thickness to be used in Monte Carlo simulation programs to produce a satisfactory result. With recourse to the analytical formula, however, it was possible to parameterize the central and intermediate region sizes, as well as their dead layer thicknesses, which facilitated the application of the least-squares method to obtain the calibration function.

The efficiency calibration curve was based on the experimental efficiency values determined from the spectra taken with the calibration sources, completed with information obtained from detector characteristics. The least-squares procedure must take into account the correlations between the experimental efficiency data, and the correct calculation of χ^2 requires the full variance matrix given by formula (15). One of the consequences of these correlations is that almost all uncertainty bars are crossed by the fitted curve, as can be seen in Figs. 5 and 7.

In the case of this experiment, two detector arrangements were used, differing only in the use (or not) of a broad-angle collimator. This means that the thin dead-layer thickness is the same in both efficiency calibrations, and there are three different ways to determine this parameter: fitting it to any of the two efficiency data sets or to both data sets in a single least-squares procedure. The last method is more precise in principle, because it uses all available data, but it is also more involved. We performed all the three procedures, and found values in complete agreement with the results shown in the previous section. The simultaneous fit of the efficiencies in both experimental arrangements gave dead-layer thicknesses and solid angles with slightly smaller standard deviations, as expected. Using the uncollimated data only, the *standard deviation* in the central region dead-layer thickness, d_{thin}, was much larger than that obtained from the model fit to the collimated data.

The measurement of the intermediate dead-layer thickness relying on the 2- and 1-mm collimator scan data are marginally compatible with the results obtained with the least-squares fitting procedure. The existence of transition layers between the active and dead layers in large detectors has been recently observed [1]. Since this question is outside the scope of this paper, we added an appendix with all our results concerning the direct measurement of dead layers from photon attenuation, which suggest that a similar phenomenon may be happening in this small detector.

Although developed for pin-hole photon beams, Seltzer's model applied well to the arrangement described in this paper. The large source-to-detector distance ensured an almost perpendicular incidence of the photon beam on the crystal surface, which seems to be the necessary condition for the validity of this model. At closer geometries, it might be necessary to take the beam divergence into account, as recommended for measurements with Si(Li) detectors [25].

Since we did not have any experimental data below the Ge K binding energy, 11 keV, we did not try to apply the model in this energy region. In fact, the 50 μm Al window employed in our experimental arrangement is a significant attenuator for these low-energy photons, thus this window alone plays a role in the detection efficiency which is much more important than the other factors included in the efficiency model; in the energy range considered here, the Al window caused the slight tilt observed in the efficiency plateau around 50 keV (see Fig. 5). Therefore, although Seltzer's model likely applies for energies below 11 keV, testing it requires thinner spectroscopy windows.

7. Conclusions

The efficiency model given by formulas (11) and (8) based on Seltzer's analytical model [17] was able to fit adequately the experimental values and is in complete agreement with our experimental observations. It was shown that a properly placed collimator assures good detector response, as already pointed out by Martin and Burns [12], which confirmed that the crystal frontal dead layer was still thin in the central region despite the thick dead layer that developed near the detector rim. With Seltzer's analytical model, a HPGe x-ray detector with an uniform dead-layer can be calibrated in efficiency for sources placed in far geometry using only ^{57}Co.

It was found that the planar HPGe x-ray detector studied in this work has a guard-ring that was insufficient to assure a constant efficiency with time. Since the guard-ring size is not disclosed by the manufacturers and seldom stated in the detector data sheet, it is important that the experimentalist pays attention to the signs pointing to the development of significant dead layers in the detector region responsive to x-rays, which may happen more often than desirable. The main practical nuisance of these dead layers is that the hypothesis that the full-energy peak efficiency is well represented by a single plateau curve must be regarded with caution; although it is possible to find an appropriate analytic formula, as it was described in this paper, and to gather a set of calibrated radioactive sources that give a sufficient number of data points to obtain a reliable fit, these are time-consuming tasks that would be better avoided. Therefore, we are adding the following steps to our routine of efficiency calibration of planar HPGe x-ray detectors:

- Take an x-ray image from the detector to check the crystal alignment and guard-ring size. In such an image we could observe that the crystal was tilted and not placed where it was supposed to be. This is important not only in the determination of geometrical characteristics of the experimental arrangement, like angles in angular distribution measurements, but also to correctly place a collimator.
- Measure the distance between source and crystal frontal surface and check if the maximum efficiency is greater than 0.92 of the subtended solid angle.
- Check the efficiency curve for bumps around 80 keV.
- Check for an increased proportion of events in the continuum of the energy spectrum with respect to the full-energy peak; refer to Martin and Burns [12] for further details.

When signs of a dead layer in the region not covered by the detector internal collimator are noticed, the use of an appropriate external broad-beam collimator that limits the photon flux to a thin dead layer central region may render the efficiency calibration simpler.

Our results of the Ge crystal frontal surface scanning with pencil beams, along with information scattered in the literature, allowed us to propose a detector model, based on Seltzer's analytical model, which explained the peculiar dependence of the HPGe x-ray efficiency with energy observed in our experiment. Changes of Ge crystal dead layer thickness have consequences in the efficiency of x-ray detectors that may not be remarkable at first sight but nevertheless require particular attention from the experimentalists.

Acknowledgments

The authors gratefully acknowledge financial support from the FAPESP (Fundação de Amparo à Pesquisa do Estado de São Paulo, Brazil) Contract numbers 2010/52616-7 and 2010/19699-6, the MICINN (Ministerio de Ciencia e Innovación, Spain) Project no. FPA2009-14091-C02-01 and the DFG (Deutsche Forschungsgemeinschaft) project BR 4043/1-1. Support from CAPES (Coordenação de Aperfeiçoamento de Pessoal de Ensino Superior, Brazil) and CNPq (Conselho Nacional de Pesquisas, Brazil) is also acknowledged. The authors are grateful to M.Sc. Martha A. Aldred for the radiographic images, to Dr. Marina F. Koskinas for the calibrated sources and to Dr. Daniel R. Napoli for enlightening discussions.

Appendix A. Steepness of the boundary between thin and thick dead-layer regions in Ge crystal

The photon beam scan of the Ge crystal surface with the ^{241}Am source and the 2-mm collimator showed that the 14–59 keV photon intensity ratio was constant over the crystal surface, suggesting a sharp change in dead-layer thickness. A more detailed scan, with a 1 mm collimator, unveiled a more complicated pattern. Nevertheless, the 14- to 59-keV ratio was still fairly constant over the surface whenever the 14 keV x-ray was observed. In this appendix, we will model the dead-layer shape and place bounds on the steepness of change in its thickness, based on the experimental data we have obtained.

The quantities that we are going to model are the ratios of the 14 keV and 59 keV peak areas to their values in the central region, determined using formula (2) in the text, and named $R_{14,k}$, and $R_{59,k}$, where k identifies the position on the crystal surface. Table A1 lists these ratios for the pixels where the 14- and 59-keV peak areas differed from that of the central region, in the measurement with the narrow, 1 mm, collimator. We can check that the ratio $R_{59,k}/R_{14,k}$ is fairly constant and approximately equal to 1, which is quite unexpected and points to an abrupt change in dead-layer thickness.

Table A1
Columns 1 and 2 give the ratio between intensity in one of the borderline pixels to the average intensity in central region, for 14 and 59 photons from ^{241}Am, respectively. Columns 3 and 4 give r_{thin} calculated by formula (A.1), in mm, using the experimental ratios given in columns 1 and 2, respectively.

$R_{E,i}=A_{E,i}/\langle A_{E,c}\rangle$		r_{thin} with $\delta=0$	
14 keV	59 keV	14 keV	59 keV
0.544(23)	0.555(7)	0.04(4)	0.013(8)
0.891(23)	0.860(9)	0.30(5)	0.290(9)
0.224(22)	0.257(5)	−0.20(4)	−0.253(12)
0.333(24)	0.379(6)	−0.10(4)	−0.140(10)
0.708(23)	0.679(8)	0.14(4)	0.120(8)
0.618(24)	0.604(8)	0.08(4)	0.055(8)
0.794(23)	0.808(9)	0.25(4)	0.238(9)
0.388(24)	0.375(6)	−0.10(4)	−0.143(10)

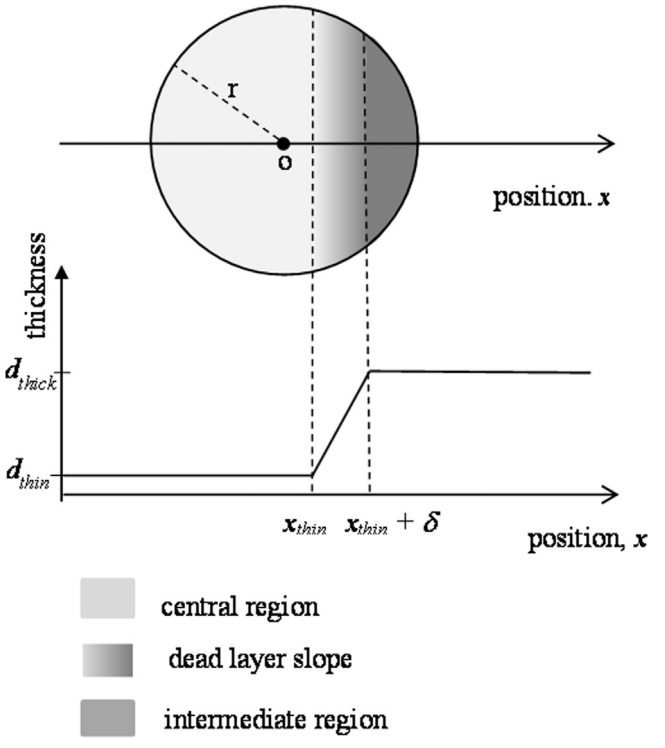

Fig. A1. The circle represents the pixel on the crystal surface, with radius $r=0.50$ mm, where the two vertical lines show the onset and end of the transition in dead layer thickness. The graph shows the thickness function adopted in the model.

Fig. A1 depicts the detector pixel hit by the photon beam, with radius r, on the boundary between the central and intermediate regions, as well as the dead-layer depth function model, where we assumed for simplicity that the change in thickness happens at a constant rate, along a distance δ. We assume also that δ is sufficiently small for the transition between the thin and thick dead-layers to be bounded within one pixel. Since the pixel radius is much smaller than the crystal radius, the transition between regions was considered as straight lines within the pixel, as shown in Fig. A1. With these assumptions, the ratio given by Eq. (2) for a parallel monochromatic photon beam of energy E, after traversing the dead layer, is given by

$$R(E, r_{\text{thin}}, \delta, r; \Delta) = \frac{2}{\pi r}\left[\int_{-r}^{r_{\text{thin}}} \sqrt{r^2-\rho^2}\, d\rho + \int_{r_{\text{thin}}}^{r_{\text{thin}+\delta}} \exp\left(-\mu(E)\Delta\frac{\rho-r_{\text{thin}}}{\delta}\right)\sqrt{r^2-\rho^2}\, d\rho + \int_{r_{\text{thin}+\delta}}^{r} \exp(-\mu(E)\Delta)\sqrt{r^2-\rho^2}\, d\rho\right] \quad \text{(A.1)}$$

where $\Delta = d_{\text{thick}} - d_{\text{thin}}$, and $\mu(E)$ is the total linear attenuation coefficient of photons of energy E in Ge. The first and last integrals correspond to the areas of the respective circular segments on Fig. A1, but the term in the middle has not an analytical expression, hence the integral must be evaluated numerically.

Applying formula (A.1) to this detector and the narrow collimator ($\Delta = 2.3$ mm and radius $= 0.5$ mm) to a borderline pixel k where r_{thin} is exactly at its center, the ratio $R_{59,k}/R_{14,k}$ changes from 1.08 to 1.41 when δ increases from 0 to the pixel radius, almost linearly. Therefore, a gradual increase in dead-layer thickness tends to yield ratios significantly greater than 1, which is not observed in Table A1, hence leading us to analyze the data under the hypothesis that $\delta = 0$.

The last two columns of Table A1 list the values of r_{thin} deduced from Eq. (A.1) using $\delta = 0$ and the experimental values $R_{14,k}$ and $R_{59,k}$, where the uncertainty in $\Delta = 2.3(4)$ was taken into account. We notice that r_{thin} calculated from the 59 keV γ rays is systematically smaller than that calculated from the lower energy photons by 30 μm in average.

In a recent work, the Majorana collaboration of Aguayo et al. [1] proved "the existence of a transition layer between the active region of the detector and the outer N+ contact" in large detectors, and showed that its characteristics vary with the detector production process. A similar phenomenon in this measurement with our x-ray detector, when the 59 keV γ ray is detected very near the dead-layer (less than 1 mm), would reduce the 59 keV full-energy peak efficiency and lead to the results shown in Table A1. Although the outer contact in this detector should have a different nature and planar detectors have a uniform electric field, likely stronger in average, the observed dead-layer may affect the electric field in its vicinity, and give rise to the observed effect, much less pronounced than that seen in coaxial or point contact detectors, like that studied by Aguayo et al. [1].

Another result that we can assign to an efficiency loss due to a transition layer refers to the thick dead-layer values measured using the 121 keV to 40 keV ratio. The ratio given in formula (6) in the text was calculated for 27 pixels, and using them in formula (11) gave 25 values almost uniformly distributed in the range 3.1–4.3 mm, besides 4.6 and 4.9 mm, once for each. These values are all two standard deviations above the fitted value $\hat{d}_{\text{thick}} = 2.3(4)$ mm, a result of low statistical probability. Moreover, although many of these pixels may cover partially all three detector-regions (central, intermediate, and inactive) because they are wider than the intermediate region, it is unlikely that no one correspond to the situation depicted in Fig. A1.

The detector scan with the 1-mm collimator allowed us to find a few points where the 59 keV peak from ^{241}Am was seen but not the 14 keV. The results for d_{thick} from formula (7) are 2.9, 3.4, 3.5 and 3.6 mm, all above the fitted value of $\hat{d}_{\text{thick}} = 2.3(4)$ mm. However, since the intermediate region is 1.3 mm wide according the results shown in Section 5.2, it is possible that all these pixels have some part on the crystal dead region.

The existence of a transition layer besides the dead-layer complicates the detector model and, since they cause similar effects, an ambiguity arises, whose solution is outside the scope of this paper. Overall, these results are consistent with the detector model depicted in Fig. A1 with a sharp transition in dead-layer thickness and support the efficiency model developed in this work. They also suggest the existence of a transition layer partially active for charge collection in a small, x-ray detector.

References

[1] E. Aguayo, M. Amman, F.T. Avignone, et al., Characteristics of signals originating near the lithium-diffused N+ contact of high purity germanium p-type point contact detectors, Nuclear Instruments and Methods in Physics Research Section A 701 (2013) 176.

[2] G.F. Knoll, Radiation Detection and Measurement, 3rd ed., John Wiley & Sons, 1999.

[3] P. Dryak, P. Kovar, Applied Radiation and Isotopes 64 (2006) 1346.

[4] N.Q. Huy, D.Q. Binh, V.X. An, Study on the increase of inactive germanium layer in a high-purity germanium detector after a long time operation applying MCNP code, Nuclear Instruments and Methods in Physics Research Section A 573 (2007) 384.

[5] N.Q. Huy, The influence of dead layer thickness increase on efficiency decrease for a coaxial HPGe p-type detector, Nuclear Instruments and Methods in Physics Research Section A 621 (2010) 390.

[6] K. Debertin, R.G. Helmer, Gamma and X-ray Spectrometry with Semiconductor Detectors, 3rd ed., North-Holland, Amsterdam, 1998.

[7] R.M. Keyser, W.K. Hensley, Efficiency of germanium detectors as a function of energy and incident geometry: Comparison of measurements and calculations, Journal of Radioanalytical and Nuclear Chemistry (2005) 259.

[8] M. Schläger, Precise modelling of coaxial germanium detectors in preparation for a mathematical calibration, Nuclear Instruments and Methods in Physics Research Section A 580 (2007) 137.

[9] J. Boson, G. Ågren, L. Johansson, A detailed investigation of HPGe detector response for improved Monte Carlo efficiency calculations, Nuclear Instruments and Methods in Physics Research Section A 587 (2008) 304.

[10] L. Sajo-Bohus, D. Rosso, A.M. Sajo Castelli, D.R. Napoli, E. Fioretto, R. Menegazzo, H. Barros, C.A. Ur, D. Palacios, J. Liendo, HPGe detectors long time behaviour in high-resolution ? spectrometry, Nuclear Instruments and Methods in Physics Research Section A 648 (2011) 132.

[11] K. Vetter, Recent developments in the fabrication and operation of Germanium detectors, Annual Review of Nuclear and Particle Science 57 (2007) 363.

[12] L.J. Martin, P.A. Burns, The HPGe as a defined-solid-angle detector for low-energy photons, Nuclear Instruments and Methods in Physics Research Section A 312 (1992) 146.

[13] R.G. Helmer, J.C. Hardy, V.E. Iacob, M. Sanchez-Vega, R.G. Neilson, J. Nelson, The use of Monte Carlo calculations in the determination of a Ge detector efficiency curve, Nuclear Instruments and Methods in Physics Research Section A 511 (2003) 360.

[14] C.M. Salgado, C.C. Conti, P.H.B. Becker, Determination of HPGe detector response using MCNP5 for 20–150keV x-rays, Applied Radiation and Isotopes 64 (2006) 700.

[15] R. Luís, J. Bento, G. Carvalhal, P. Nogueira, L. Silva, P. Teles, P. Vaz, Parameter optimization of a planar BEGe detector using Monte Carlo simulations, Nuclear Instruments and Methods in Physics Research Section A 623 (2010) 1014.

[16] J. Ródenas, A. Pascual, I. Zarza, V. Serradell, J. Ortiz, L. Ballesteros, Analysis of the influence of germanium dead layer on detector calibration simulation for environmental radioactive samples using the Monte Carlo method, Nuclear Instruments and Methods in Physics Research Section A 496 (2002) 390.

[17] S.M. Seltzer, Calculated response of intrinsic Germanium detectors to narrow beams of photons with energies up to, Nuclear Instruments and Methods in Physics Research Section A 188 (1981) 133.

[18] M.M. Bé, V. Chisté, C. Dulieu, et al., Table of Radionuclides (Comments on evaluation), CEA, France (1999). ⟨http://www.nucleide.org/DDEP_WG/DDEPdata.htm⟩, last accessed April 9, 2013.

[19] M.P. Unterweger, Half-life measurements at the National Institute of Standards and Technology, Applied Radiation and Isotopes 56 (2002) 125.

[20] V.R. Vanin, N.L. Maidana, N.L. Pino, et al., First experiments with the IFUSP microtron injector, in: AIP Conference Proceedings, vol. 1351, 2011, pp. 105–116.
[21] E. Yılmaz, C. Can, Photoelectron, Compton and characteristic x-ray escape from an HPGe Detector in the range 8–52keV, X-ray Spectrometry 33 (2004) 439.
[22] M.P. Fioratti, S.R. Piermattei, Calculation of the escape peak for Ge-Li and NaI radiation detectors, Nuclear Instruments and Methods in Physics Research Section A 96 (1971) 605.
[23] M.J. Berger, J.H. Hubbell, S.M. Seltzer, et al., XCOM: Photon Cross Sections Database. NIST Standard Reference Database 8 (XGAM), 2011. ⟨Http://www.nist.gov/pml/data/xcom/index.cfm⟩, last accessed March 29, 2013.
[24] L. Venturini, V.R. Vanin, HPGe detector efficiency calibration for extended sources in the 50–1400keV energy range, Applied Radiation and Isotopes 44 (1993) 999.
[25] J.M. O'Meara, J.L. Campbell, X-Ray Spectrometry 33 (2004) 146.